WHITE DWARF STANDARD STARS: G191−B2B, GD 71, GD 153, HZ 43

RALPH C. BOHLIN AND LUIS COLINA[1]
Space Telescope Science Institute, 3700 San Martin Drive, Baltimore, Maryland 21218
Electronic mail: bohlin@fos.stsci.edu, colina@stsci.edu

DAVID S. FINLEY
Center for EUV Astrophysics, 2150 Kittredge Street, University of California, Berkeley, California 94720
Electronic mail: david@cea.berkeley.edu

Received 1995 May 1; revised 1995 May 25

ABSTRACT

Three additional white dwarfs, GD 71, GD 153, and HZ 43, covering a wide range in effective temperature, have been observed with *HST* faint object spectrograph (FOS) to check the G191−B2B white dwarf based absolute calibration of *HST* instruments. The FOS spectrophotometry of the three additional white dwarfs agree with model spectra to ~2%. The FOS absolute flux of G191−B2B, GD 71, and GD 153 agree with Landolt photometry to better than 1% on average, in *B* and *V*. Consequently, the white dwarfs G191−B2B, GD 71, GD 153, and HZ 43 are the primary reference standards that are recommended for all ultraviolet and optical absolute calibrations from 1000 to 10 000 Å. © *1995 American Astronomical Society.*

1. INTRODUCTION

Starting with cycle 4 in 1994 January, the calibrated absolute flux of the *HST* instrument complement has been on a preliminary white dwarf (WD) scale (Bohlin 1994; Bohlin & Colina 1994; Finley 1994). This WD scale has a relative flux distribution that is defined by a preliminary pure hydrogen model atmosphere with $T_{\rm eff}$=60 000 K and log g=7.50 for G191−B2B. Recently, Finley *et al.* (1995) derive an improved $T_{\rm eff}$=61 300 K, which makes the far-UV flux of the model 1.5% brighter at 1200 Å with respect to 5490 Å. The absolute flux scale is determined by *V* band photometry from Landolt (Colina & Bohlin 1994). In the case of the faint object spectrograph (FOS), the absolute calibration is determined by direct observation of G191−B2B. For other *HST*

TABLE 1. *HST* WD standards. Astrometry.

Star (1)	α(2000) (2)	δ(2000) (3)	μ_α (4)	μ_δ (5)	Ref. (6)	GSC No. (7)	GS Region (8)	Plate ID (9)	Epoch (10)
G191-B2B	05:05:30.62	+52:49:54.0	+0.0008	−0.0873	1	3734−506	N119	0005	1983.12
GD 71	05:52:27.51	+15:53:16.6	+0.0047	−0.1879	2	–	N418	009N	1982.96
GD 153	12:57:02.37	+22:01:56.0	−0.0015	−0.1898	3	1455−1145	N378	01PN	1982.38
HZ 43	13:16:21.99	+29:05:57.0	−0.0116	−0.0813	1,4	1996−1402	N322	002K	1982.39

Notes to TABLE 1

Explanation of the columns (1) G191-B2B has the alternative name WD0501+527 in the HST data archive; (2-3) J2000 coordinates from the STScI Guide Star Selection System; (4) proper motion in right ascension, where the motion in right ascension on the sky in seconds of arc per year is $15\mu_\alpha cos\delta$. For HZ 43 the value listed is the mean of the two references indicated in column six; (5) proper motion in declination in seconds of arc per year. For HZ 43 the value listed is the mean of the two references indicated in column six; (6) reference for proper motion; (7) Guide Star Catalogue number of the standard star; (8) Guide Star Selection System field number; (9) Guide Star Selection System plate number; (10) date plate was exposed.

References: (1) Harrington & Dahn 1980; (2) Giclas, Burnham & Thomas 1980; (3) This work where the proper motion has been measured using the Guide Star System and plates at two different epochs separated by 26 years; (4) Lang 1992.

[1]On assignment from the Space Science Department of ESA.

 0004-6256/95/110(3)/1316/10/$0.90

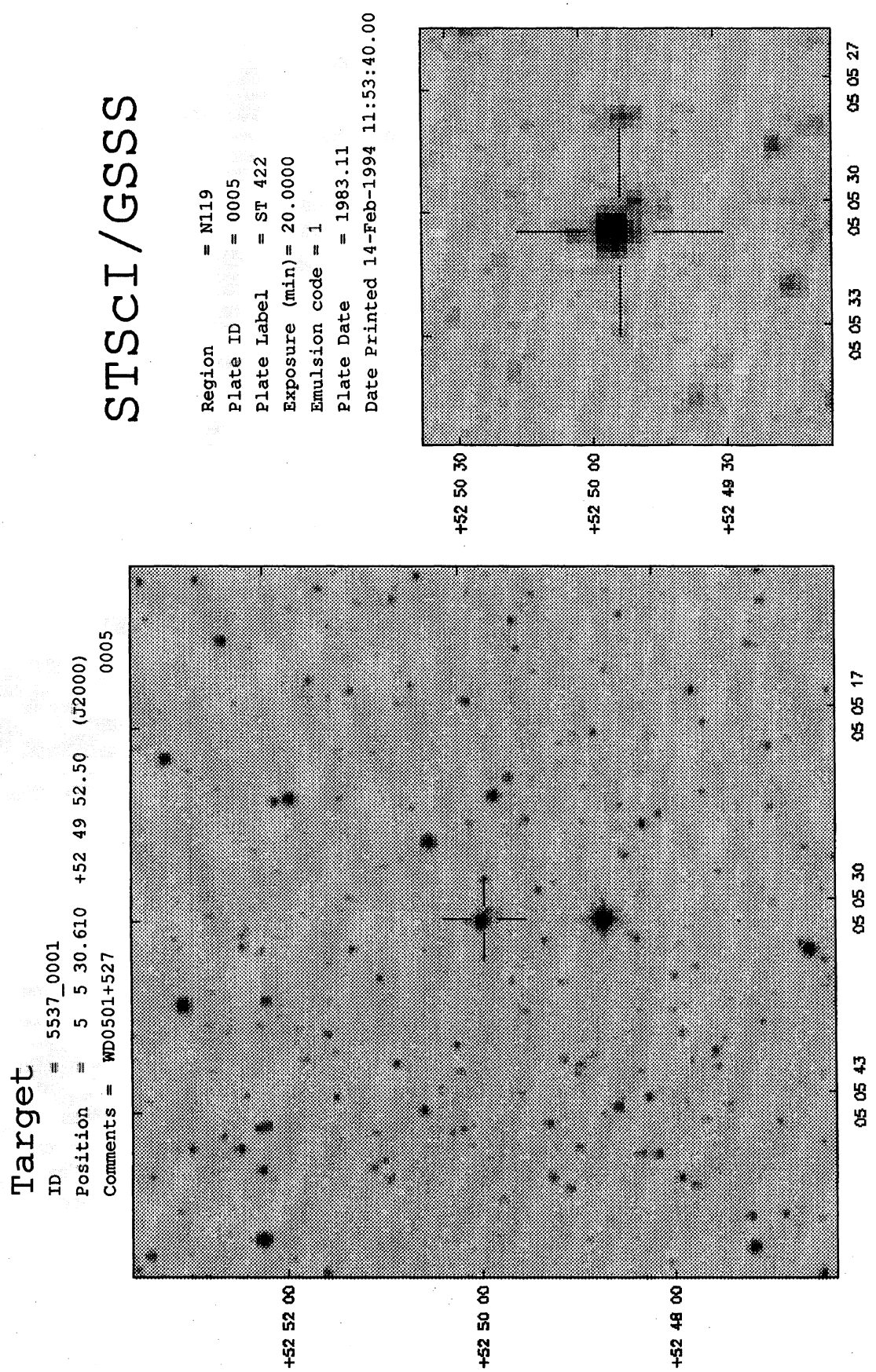

FIG. 1. STScI Guide Star System finding charts for G191−B2B (WD 0501+527), GD 71, GD 153, and HZ 43. The field frame is 7.15 arcmin square, and the magnified frame is 85 arcsec square. Targets with appreciable proper motion will not be centered in the crosshairs of the chart, because the cursor is located at the predicted position for the epoch 2000.

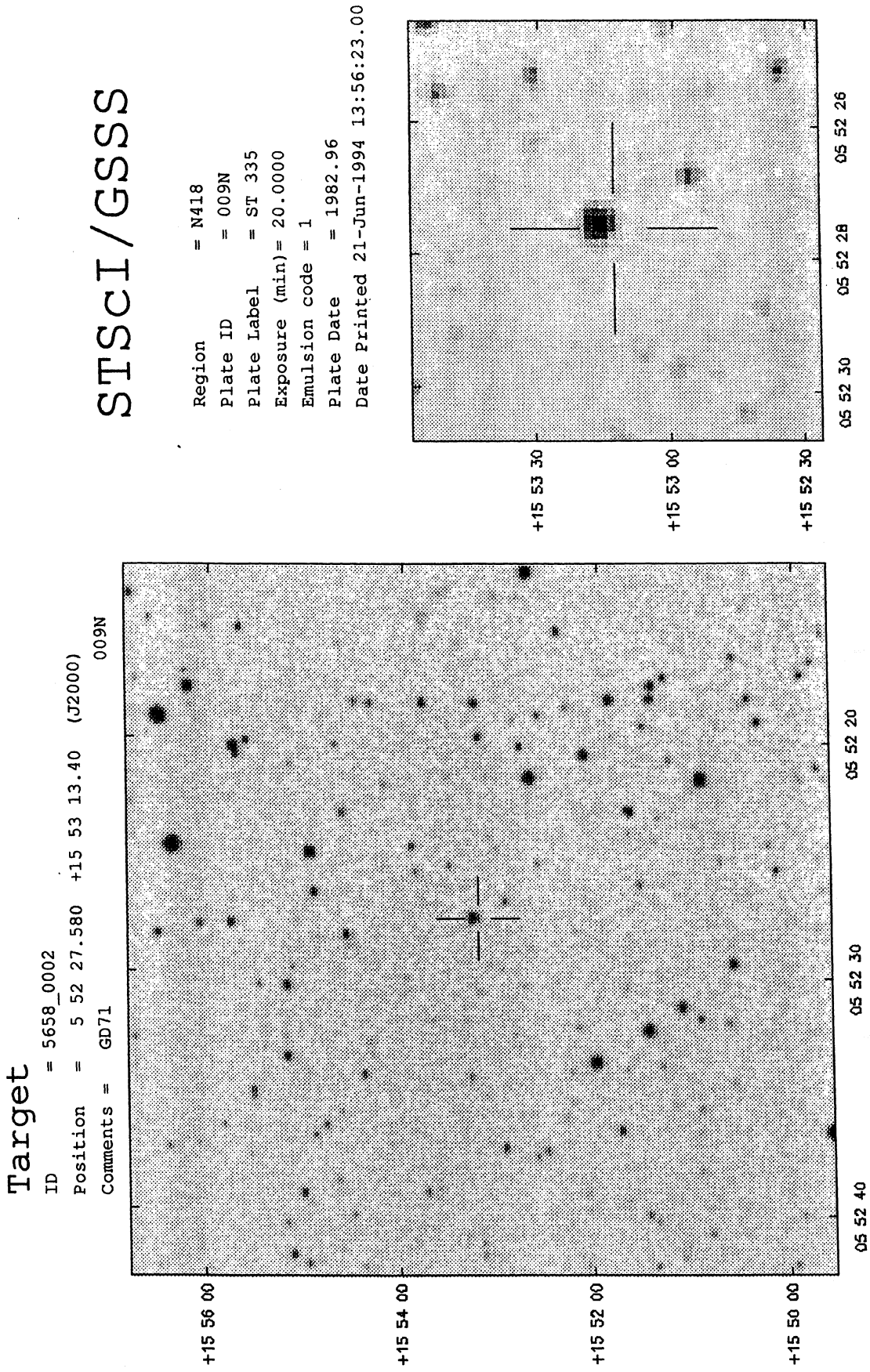

FIG. 1. (continued)

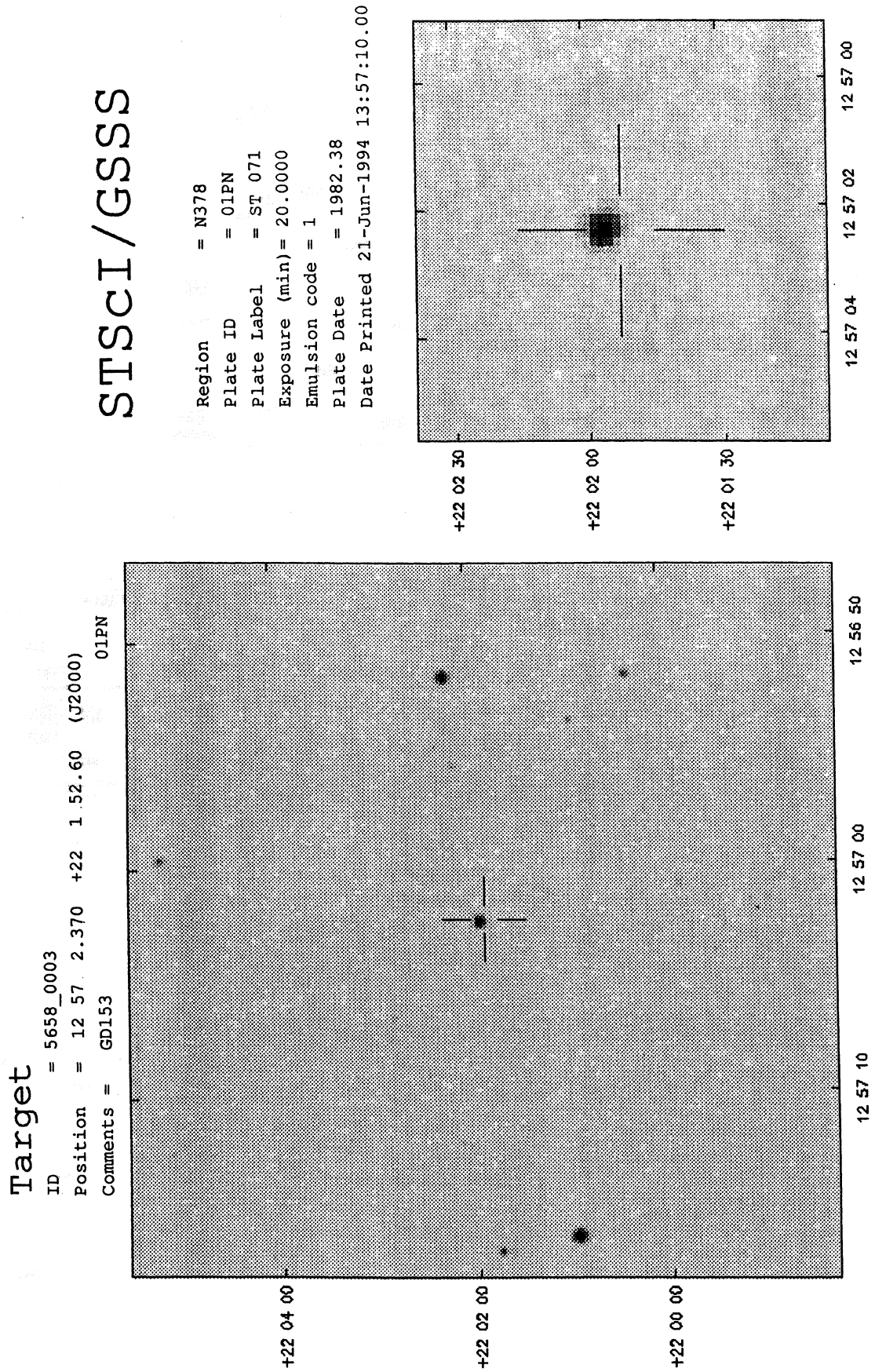

FIG. 1. (continued)

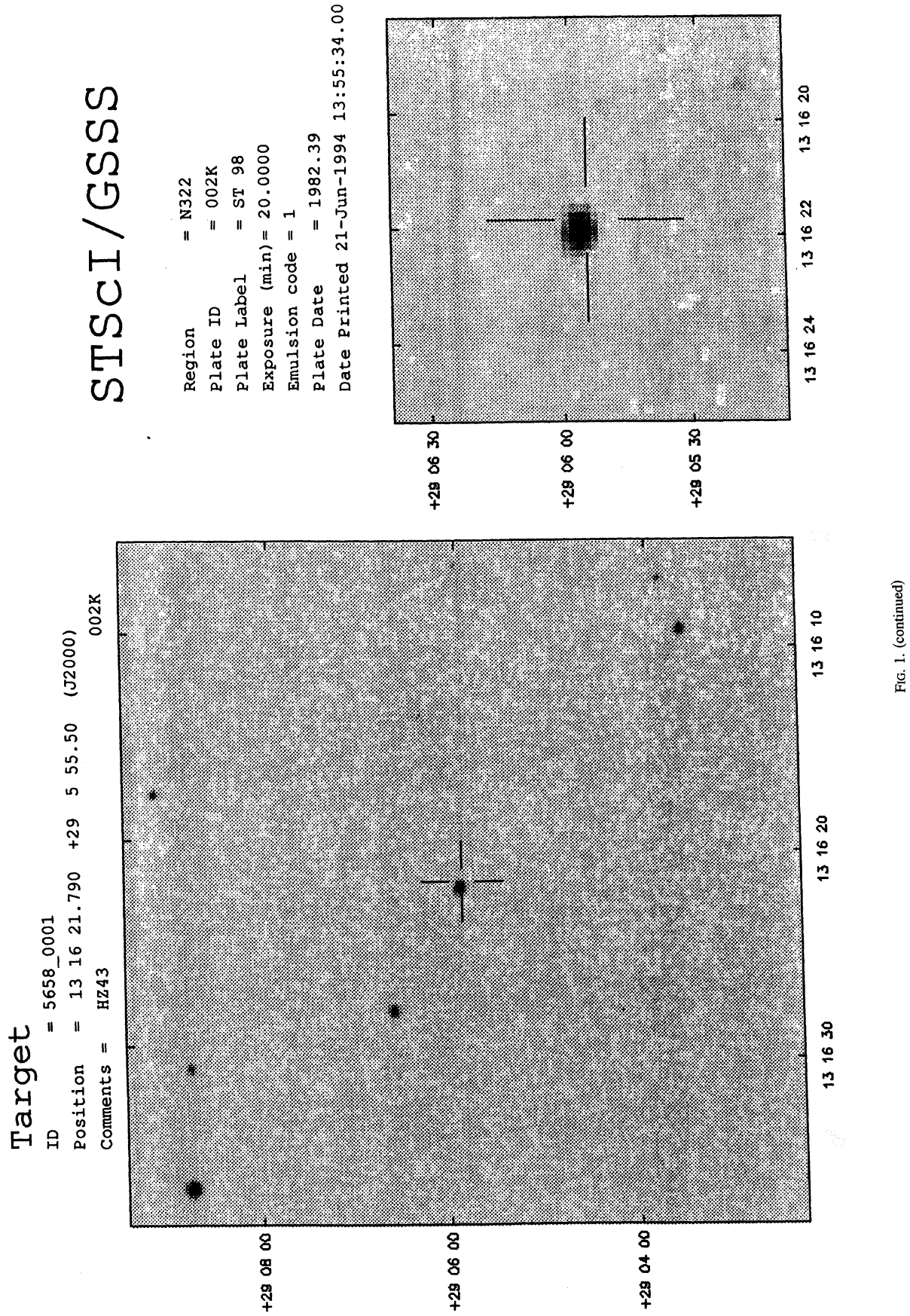

FIG. 1. (continued)

TABLE 2. Observing log of FOS/CAL proposal 5658.

Star	Intrument	Aperture	Grating	Date	Exp. Time (sec)
GD 71	FOS/BL	B-3	G130H	Aug. 20, 1994	150
			G190H	and	120
			G270H	Oct. 15, 1994	120
			G400H		120
GD 71	FOS/RD	B-3	G190H	Oct. 08, 1994	120
			G270H	and	120
			G400H	Mar. 09, 1995	120
			G570H		210
			G780H		360
GD 153	FOS/BL	B-3	G130H	Dec. 29, 1994	240
			G190H	and	120
			G270H	Mar. 02, 1995	120
			G400H		195
GD 153	FOS/RD	B-3	G190H	Jan. 02, 1995	120
			G270H	and	120
			G400H	Feb. 25, 1995	120
			G570H		420
			G780H		600
HZ 43	FOS/BL	B-3	G130H	Aug. 08, 1994	120
			G190H	and	120
			G270H	Dec. 29, 1994	120
			G400H		120
HZ 43	FOS/RD	B-3	G190H	Aug. 15, 1994	120
			G270H	and	120
			G400H	Dec. 28, 1994	120
			G570H		240
			G780H		300

instruments, a transformation of the fluxes of their observed standard stars to the WD scale is required (Bohlin 1994; Bohlin 1995 in preparation).

Section 2 describes the FOS observations of the three additional white dwarfs. Section 3 details the pure hydrogen models and the procedure used to put the model spectra on an absolute flux scale. Section 4 describes the accuracy of the FOS spectrophotometry by comparing the FOS spectra with the models and with Landolt's photometry. Section 5

TABLE 3. Characteristics of the WD models.

Star	Spec. Type	V	Ref.	Teff	log g
(1)	(2)	(3)	(4)	(5)	(6)
G191-B2B	DA0	11.781	1	61300	7.50
GD 71	DA1	13.032	2	32300	7.73
GD 153	DA1	13.346	1	38500	7.67
HZ 43	DA1	12.914	3	50000	8.00

Notes to TABLE 3

Explanation of columns:

(3) V magnitude to which models have been normalized from reference in column (4); V magnitudes are for Landolt's bandpass and sensitivity.

(5) T_{eff} in K, and (6) log g for our WD models.

References:

(1) Landolt 1994, private communication.

(2) Landolt 1992.

(3) This work using synthetic photometry on the FOS spectrum.

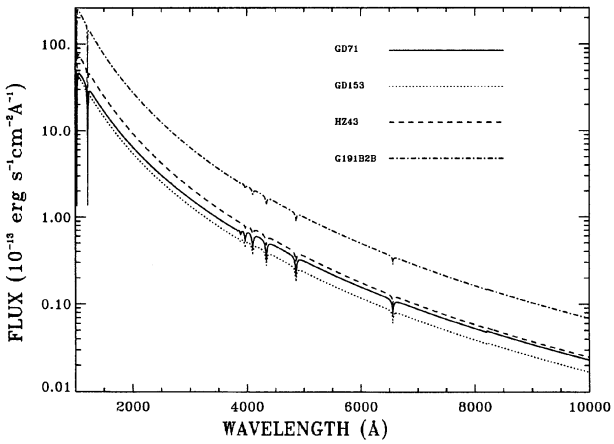

FIG. 2. Absolute flux distributions of the four pure hydrogen model flux distributions that provide the primary *HST* flux reference scale.

explains where to obtain digital versions of the absolute flux distributions for the white dwarf models.

2. OBSERVATIONS OF WHITE DWARF STANDARDS

Three additional white dwarf stars, GD 71, GD 153, and HZ 43, were observed in *HST* cycle 4 with the high dispersion modes of FOS in order to verify the consistency of the *HST* WD scale over a range of temperatures for three more stars with pure hydrogen atmospheres. The selection criteria required (1) a range of effective temperatures, (2) a high flux to minimize *HST* observing time, (3) a negligible interstellar extinction (Vennes *et al.* 1994), and (4) a zero metallicity, as verified by EUV observations.

The astrometric parameters and field charts used in the *HST*/FOS observations of the three additional white dwarfs, plus G191−B2B, are presented in Table 1 and Fig. 1, respectively. All FOS observations of the additional white dwarfs used the B−3 (0.86″) aperture. The targets were acquired using a four-stage peakup acquisition procedure. The journal of the observations is in Table 2.

3. PURE HYDROGEN MODELS OF WHITE DWARF STANDARDS

The three white dwarfs are modeled by pure hydrogen atmospheres characterized by the effective temperatures and gravities listed in Table 3. $T_{\rm eff}$ and log g are derived from detailed fits to the Balmer line profiles using high S/N optical spectra of these stars obtained by Finley. As for G191−B2B, the comparison model fluxes were calculated using Detlev Koester's white dwarf model atmosphere codes. Koester's models are described in Koester *et al.* (1979). A more complete description of the optical observations, Balmer fitting procedure, and a description of the models will be presented in Finley *et al.* (1995).

The uncertainties in the predicted fluxes due to uncertainties in the models or in the derived stellar parameters are small. The stars are all hotter than 30 000 K; and the Balmer and Paschen continuua are on the Rayleigh–Jeans tail. Thus, the effects of errors on the slopes of the spectra are mini-

mized. The largest uncertainties are in the coolest star of the sample, GD 71. For this object, the formal 1σ error in the $T_{\rm eff}$ determination is 100 K, while a 200 K difference in $T_{\rm eff}$ changes the flux at 1150 Å relative to that at 5490 Å by only 0.7%. This difference monotonically decreases toward longer wavelengths, except in the lines, where a maximum difference of 4% is seen at the center of the Lyα line. Differences within the Balmer lines are all less than 1%.

The 1σ uncertainty in $\log g$ is 0.03 dex, but changing $\log g$ by twice that amount only changes the relative con-

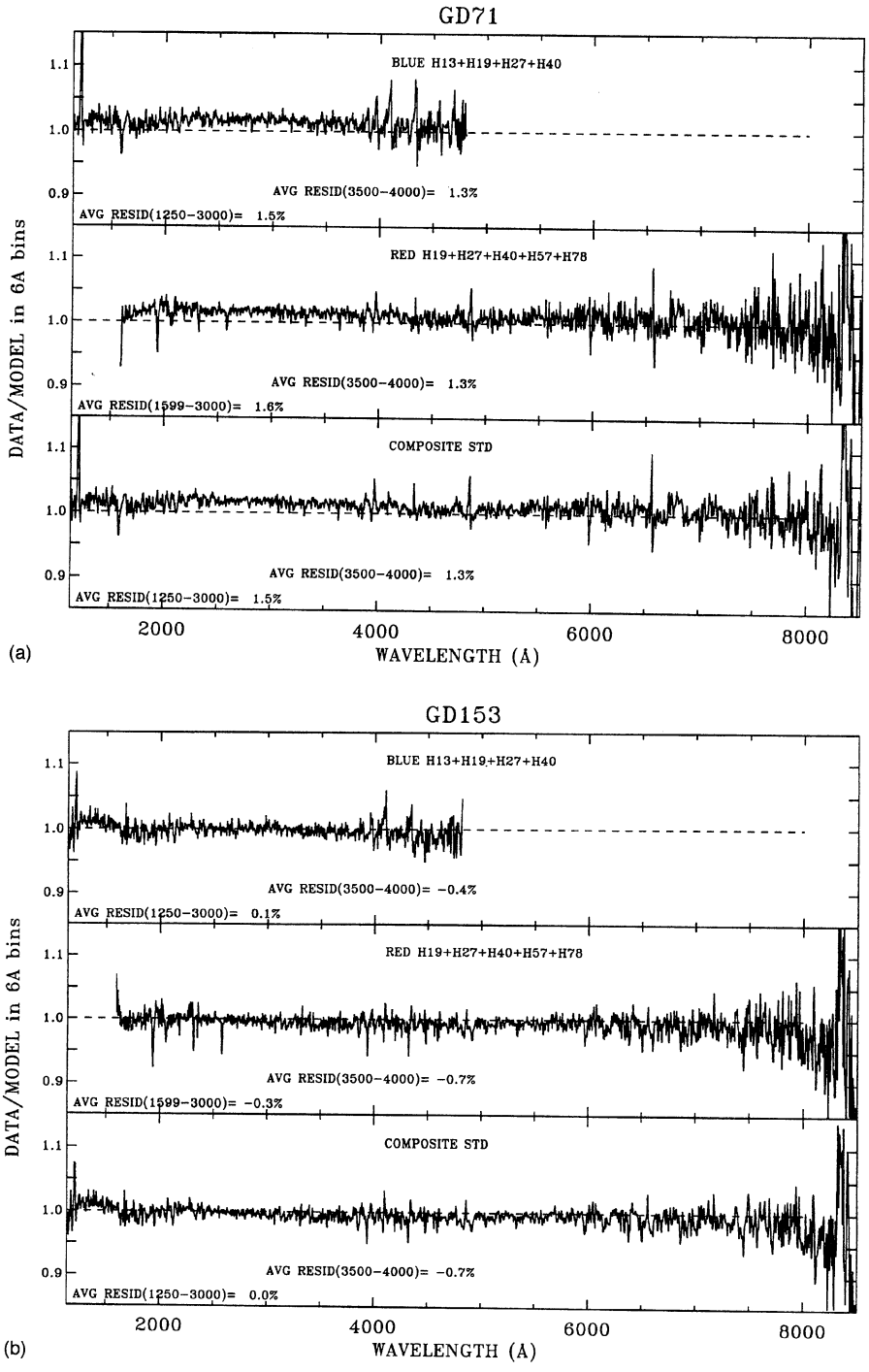

FIG. 3. Ratios of FOS fluxes to the pure hydrogen model atmospheres in 6 Å bins. Top panels: FOS blue side high dispersion gratings H13, H19, H27, and H40. Middle panels: FOS red side high dispersion gratings H19, H27, H40, H57, and H78. Bottom panels for GD 71, GD 153, and HZ 43 in (a)–(c). Best composite FOS spectrum, with blue side data shortward of 2600 Å and red side data longward of 2600 Å. Bottom panel for G191−B2B in (d). Composite spectrum of blue side 1140–2085 Å, red side 2085–3300 Å, blue side 3300–3850 Å, and Oke spectrum longward of 3850 Å, where the main residuals are in the hydrogen lines and in the circumstellar C IV at 1550 Å and Mg II at 2800 Å. Data from *HST* cycles 1–4 are included in Fig. 3(d).

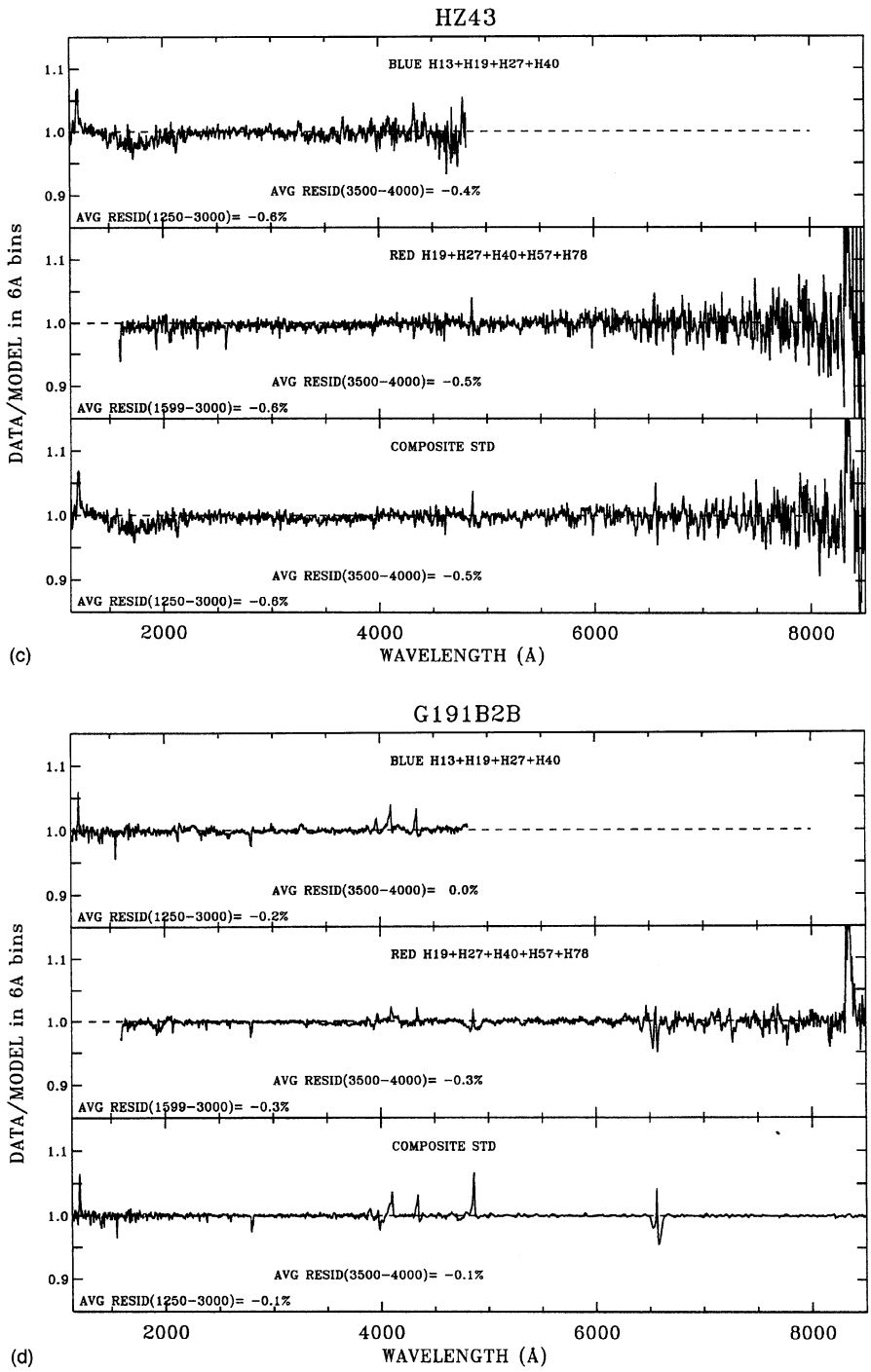

FIG. 3. (continued)

tinuum fluxes by 0.2%. Differences in the lines exceed 0.5% only in the core of Lyα, where the difference is 5%.

One uncertainty in the modeling is the parameterization of the Hummer–Mihalas occupation probability formalism (Hummer & Mihalas 1988). Our models are calculated for an assumed critical field strength of twice the nominal value, to achieve consistent fits to all Balmer lines as suggested by Bergeron (1992). Assuming the nominal value would give $T_{\rm eff}$=31 900 K, log g=7.69, compared to our adopted parameters of $T_{\rm eff}$=32 300 K and log g=7.73. The differences between the two models are <2% in the red wing of Lyα, 5% in Lyα, <1% longward of 1250 Å, and barely exceeds 1% between high Balmer lines.

The models are placed on an absolute flux scale using the

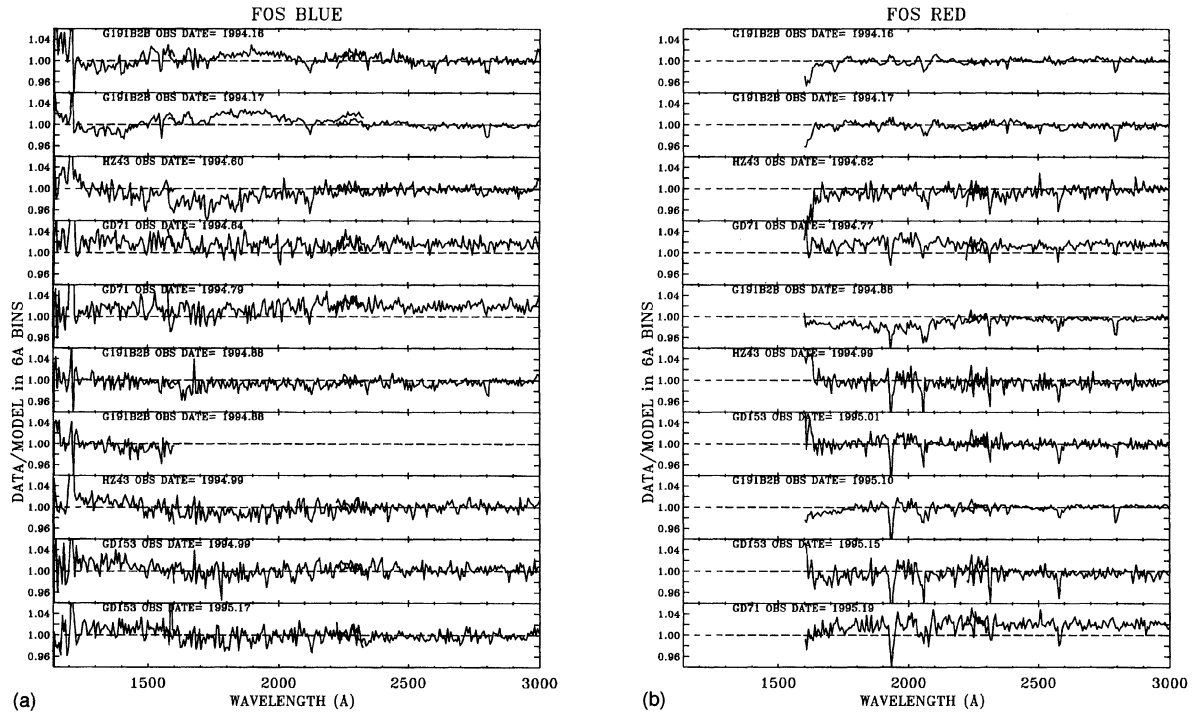

FIG. 4. Residuals as in Fig. 3 for the individual cycle 4 observations, where time of observation increases from top to bottom. The broad systematic deviations of 2%–3% from unity are the intrinsic limits to FOS photometric precision. However, the first two blue side observations of G191−B2B demonstrate a much better repeatability that is often seen for FOS over short intervals of a few days.

V magnitudes in Table 3 and the technique of Colina & Bohlin (1994). Figure 2 shows the adopted absolute fluxes for the additional WD standard stars along with G191−B2B.

4. FOS ABSOLUTE SPECTROPHOTOMETRY

4.1 FOS Spectra Versus Models

Figure 3 shows the ratio of the fluxes of the co-added FOS spectra to the corresponding models for the blue side, red side, and best combined FOS data. There are narrow glitches in the ratios because of small differences in Balmer line profiles, Geocoronal Lyα, and residual flat-field features on the red side. The flat fielding should improve after accounting for the changes with time of the red side flats for H19 and H27. In Fig. 3(d) for G191−B2B, the extensive cycle 1–3 observations have been combined with the cycle 4 data to produce a high S/N FOS spectrum; and the even higher S/N data of Oke (1990) are used longward of 3850 Å. Since the G191−B2B model defines the absolute flux scale for FOS calibration and since the Oke spectrum has been corrected to the flux distribution of the model with a smooth spline fit, the only differences between model and data for G191−B2B are in the narrow features.

The 500-Å-wide dip of almost 3% at 1750 Å in Fig. 3(c) for HZ 43 is probably a 2–3 sigma statistical effect at the limit of the FOS photometric repeatability. Figure 4 shows the individual cycle 4 observations that are included in the data used for Fig. 3. Figure 4(a) demonstrates that neither observation of HZ 43 differs more from unity than the first two ratios for G191−B2B. More FOS observations of the three new white dwarf standards are needed to verify the flux distributions to the 1% level.

TABLE 4. FOS vs Landolt photometry.

Star	V_S^1	B_S^1	V_S-V^2	B_S-B^2	Offset
G191-B2B	11.783	11.450	+0.002	−0.005	−0.0015
GD 71	13.023	12.771	−0.009	−0.012	−0.0105
GD 153	13.352	13.071	+0.006	+0.011	+0.0085
HZ 43*	12.914	12.602	+0.030	+0.020	+0.0250

Notes to TABLE 4

[1] V_S and B_S are the synthetic Landolt photometry from FOS spectra.
[2] V and B indicate Landolt's measurements.
* HZ43 has a red close companion that is within Landolt's aperture; and section 4 explains how we have corrected his photometry for the companion.

4.2. FOS Versus Landolt Broadband Photometry

One more check of the FOS spectrophotometry is provided by the comparison of the synthetic broadband photometry of the FOS spectra with Landolt's *B* and *V* magnitudes. Following the method outlined in Colina & Bohlin (1994), *B* and *V* Landolt magnitudes for the FOS spectra of all four white dwarfs are computed (V_S and B_S in Table 4). The absolute scale of the FOS spectra of G191−B2B, GD 71,

and GD 153 agrees with Landolt's photometry (V and B in Table 4) to better than 1%, for all three of the single isolated stars.

For HZ 43, direct comparison with Landolt photometry is complicated by the red, close companion, which is separated by only ~3″ (Luyten 1970; Napiwotzki *et al.* 1993). Landolt's V and B magnitudes for HZ 43 have been obtained from recent photometric measurements using an aperture of 17.7 arcsec centered on HZ 43 (Landolt, private comm.). Consequently, the HZ 43 companion contributes to the V and B magnitudes measured from the ground. Long-slit spectroscopic ground-based observations provide the separate spectra for HZ 43 and its companion (Napiwotzki *et al.* 1993). Synthetic photometry performed on the optical HZ 43 spectrum and on the combined HZ 43+companion spectrum, demonstrates that the HZ 43+companion spectrum is 0.24 and 0.03 mag brighter than HZ 43 in V and B, respectively. These corrections are applied to Landolt's photometry, and our results indicate that the FOS V and B photometry agrees with Landolt's corrected values to 2%–3% (see Table 4). Because of the uncertainty of this correction procedure, the FOS magnitude for HZ 43 appears in Table 3 and is used to set the absolute flux scale for the HZ 43 model.

5. PUBLIC ACCESS TO DIGITAL SPECTRA OF THE STANDARDS

The fluxes of the white dwarf models, together with those of the rest of the *HST* calibration standards, can be found in UNIX SDAS binary table format on the world wide web with the URL identifier http://www.stsci.edu/ftp/cdbs/calspec. Filenames are*_mod_001.tab, where * indicates the name of the star. On the VMS STScI science cluster, the same data can be found in disk$calibration: [cdbsdata.refer.calspec]*_mod_001.tab. Any future updates to the model flux distributions will have the same root name, except that the 001 will be incremented.

6. SUMMARY

Whenever possible, one of the four white dwarf standards should be observed to determine the best instrumental calibrations on the WD scale. Finding charts from the STScI GSSS appear in Fig. 1 and can be compared to similar figures for G191−B2B and GD 71 in Turnshek *et al.* (1990). However, caution is required for ground-based observations of HZ 43 because of the red companion at ~3″ (Luyten 1970; Napiwotzki *et al.* 1993). More FOS observations of the three new white dwarfs are needed to derive the white dwarf based FOS calibration to greater precision. Additional work on the inclusion of metals in the model atmosphere calculations for G191−B2B is needed, since Sion *et al.* (1992) have shown that absorption in metal lines is important at the 2% level in some wavelength regions.

More work on the model atmospheres is required from 1 to 2.5 μm, in order to provide primary WD flux standards for the calibration of NICMOS, the future *HST* infrared camera that is planned for the 1997 servicing mission.

We thank Dr. Napiwotzki who generously provided the optical spectra of HZ 43 and companion. The authors also thank Dr. A. Landolt for providing us with accurate new photometry for GD 153 and HZ 43. This work is based on observations with the NASA/ESA *Hubble Space Telescope*, obtained at the Space Telescope Science Institute, which is operated by AURA, Inc. under NASA Contract No. NAS5-26555.

REFERENCES

Bergeron, P. 1992, in White Dwarfs: Advances in Observation and Theory, NATO ASI series, edited by M. A. Barstow (Kluwer, Dordrecht), p. 267
Bohlin, R. C. 1994, in Proceeding Conference on Calibrating HST, p. 234; also CAL/SCS-002
Bohlin, R. C., & Colina, L. 1994, HST Newsletter 11, 17
Cheselka, M., Holberg, J., Watkins, R., Collins, J., & Tweedy, R. 1993, AJ, 106, 2365
Colina, L., & Bohlin, R. C. 1994, AJ, 108, 1931
Finley, D. S. 1994, in Proceeding Conference on Calibrating HST, p. 416
Finley, D. S., Koester, D., & Basri, G. 1995, in preparation
Giclas, H. L., Burnham, R., & Thomas, N. G. 1980, Lowell Obs. Bull. No. 166, 157
Harrington, R. S., & Dahn, C. C. 1980, AJ, 85, 454
Hummer, D. G., & Mihalas, D. 1988, ApJ, 331, 794
Koester, D., Schulz, H., & Weidemann, V. 1979, A&Ap, 76, 262
Landolt, A. 1992, AJ, 104, 340
Lang, K. R. 1992, Astrophysical Data: Planets and Stars
Luyten, W. J. 1970, White Dwarfs (University of Minnesota Press, Minneapolis)
Napiwotzki, R., Barstow, M., Fleming, T., Holweger, H., Jordon, S., & Werner, K. 1993, A&Ap, 278, 478
Oke, J. B. 1990, AJ, 99, 1621
Sion, E., Bohlin, R., Tweedy, R., & Vauclair, G. 1992, ApJ, 391, L29
Turnshek, D., Bohlin, R. Williamson, R., Lupie, O., & Koornneef, J. 1990, AJ, 99, 1243
Vennes, S., Dupuis, J., Bowyer, S., Fontaine, G., Wiercigroch, A., Jelinsy, P., Wesemael, F., & Malina, R. 1994, ApJ, 421, L35